The American Journal of Pathology, Vol. 181, No. 5, November 2012

http://dx.doi.org/10.1016/j.ajpath.2012.07.030

Biomarkers, Genomics, Proteomics, and Gene Regulation

Large Oncosomes in Human Prostate Cancer Tissues and in the Circulation of Mice with Metastatic Disease

Dolores Di Vizio,*†‡ Matteo Morello,*†‡ Andrew C. Dudley,§ Peter W. Schow,¶ Rosalyn M. Adam,*† Samantha Morley,*† David Mulholland,‖ Mirja Rotinen,* Martin H. Hager,*† Luigi Insabato,** Marsha A. Moses,§ Francesca Demichelis,†††‡§§ Michael P. Lisanti,¶¶ Hong Wu,‖ Michael Klagsbrun,§ Neil A. Bhowmick,‖‖ Mark A. Rubin,‡‡ Crislyn D'Souza-Schorey,*** and Michael R. Freeman*†‡†††

From the Division of Cancer Biology and Therapeutics and the Uro-Oncology Research Program,‖‖ Samuel Oschin Comprehensive Cancer Institute, Cedars-Sinai Medical Center, Los Angeles, California; The Urological Diseases Research Center† and the Vascular Biology Program,§ Children's Hospital Boston, Boston, Massachusetts; the Departments of Surgery‡ and Biological Chemistry and Molecular Pharmacology,†† † Harvard Medical School, Boston, Massachusetts; the Dana Farber Cancer Institute Flow Cytometry Core Facility,¶ Boston, Massachusetts; the Department of Molecular and Medical Pharmacology,‖ Institute for Molecular Medicine, David Geffen School of Medicine, University of California at Los Angeles, Los Angeles, California; the Department of Biomorphological and Functional Science,** University Federico II, Naples, Italy; the Department of Pathology and Laboratory Medicine†† and the Institute for Computational Biomedicine,‡‡ Weill Cornell Medical College, New York, New York; Institute for Computational Biology,§§ Weill Cornell Medical College and the Centre for Inegrative Biology, University of Trento, Trento, Italy; the Department of Medical Oncology,¶¶ Kimmel Cancer Center, Thomas Jefferson University, Philadelphia, Pennsylvania; and the Department of Biological Sciences,*** University of Notre Dame, Notre Dame, Indiana*

Oncosomes are tumor-derived microvesicles that transmit signaling complexes between cell and tissue compartments. Herein, we show that amoeboid tumor cells export large (1- to 10-μm diameter) vesicles, derived from bulky cellular protrusions, that contain metalloproteinases, RNA, caveolin-1, and the GTPase ADP-ribosylation factor 6, and are biologically active toward tumor cells, endothelial cells, and fibroblasts. We describe methods by which large oncosomes can be selectively sorted by flow cytometry and analyzed independently of vesicles <1 μm. Structures resembling large oncosomes were identified in the circulation of different mouse models of prostate cancer, and their abundance correlated with tumor progression. Similar large vesicles were also identified in human tumor tissues, but they were not detected in the benign compartment. They were more abundant in metastases. Our results suggest that tumor microvesicles substantially larger than exosome-sized particles can be visualized and quantified in tissues and in the circulation, and isolated and characterized using clinically adaptable methods. These findings also suggest a mechanism by which migrating tumor cells condition the tumor microenvironment and distant sites, thereby potentiating advanced disease. *(Am J Pathol 2012, 181:1573–1584; http://dx.doi.org/10.1016/j.ajpath.2012.07.030)*

Prostate cancer is the second leading cause of cancer-related death in men in Western countries.[1] Understanding the biological aspects of progression to advanced, untreatable prostate cancer and identifying reliable markers to assess disease course before and after therapy remain major clinical challenges.

Supported by grants from the National Cancer Institute (K99CA131472 to D.D.V.), the NIH (R01CA143777 and R01DK57691 to M.R.F.), the US Army (W81XWH-08-1-0150 to M.R.F.), and the American Institute for Cancer Research (PDA 09A107 to S.M.).

Accepted for publication July 16, 2012.

A guest editor acted as editor-in-chief for this article. No person at Thomas Jefferson University or Albert Einstein College of Medicine was involved in the peer review process or final disposition of this article.

Supplemental material for this article can be found at *http://ajp.amjpathol.org* or at *http://dx.doi.org/10.1016/j.ajpath.2012.07.030*.

Address reprint requests to Dolores Di Vizio, M.D., Ph.D., or Michael R. Freeman, Ph.D., Division of Cancer Biology and Therapeutics, Cedars-Sinai Medical Center, 8700 Beverly Blvd, Davis Bldg, Suite 5069, Los Angeles, CA 90048. E-mail: dolores.divizio@childrens.harvard.edu or michael.freeman@cshs.org.

To migrate into surrounding tissues and metastasize, tumor cells undergo a broad range of physical and functional alterations, including cytoskeletal rearrangements and remodeling of the extracellular matrix (ECM).[2,3] Motile tumor cells assume several phenotypes, including a mesenchymal mode, in which the cells are elongated and fibroblast-like, and a distinct amoeboid mode, with less adherent properties and extensive membrane deformation.[4,5] Amoeboid movement through tissue spaces is characteristically rapid and only minimally dependent on repetitive cycles of membrane attachment and retraction to ECM.[6,7] Amoeboid behavior is less understood in molecular terms than mesenchymal motility; however, evidence indicates that this migration mode is driven by Rho GTPase-mediated actomyosin contractility.[4,8,9] A recent study from our group demonstrates that amoeboid behavior can be induced by microtubule instability caused by loss of the formin DIAPH3.[10] Silencing of DIAPH3 in prostate cancer cells and other tumor cell backgrounds results in an abrupt transition to amoeboid behavior, characterized by formation and retraction of bulky membrane protrusions, as well as increased motility, invasiveness, and metastatic potential.[10] We have also shown that prostate cancer cells exhibiting amoeboid behavior release large (approximately 1- to 10-μm diameter) membrane vesicles into the medium from pinched membrane blebs.[10,11] Notably, as demonstrated for the first time, to our knowledge, in the current study, these structures are large enough to be observed by light microscopy and quantified by several methods potentially applicable to clinical practice.

The term oncosome has been used to describe a category of tumor-derived microvesicle (TMV) that can propagate oncogenic information, including transfer of signal transduction complexes, across tissue spaces.[12,13] Oncosomes identified in patients with glioblastoma contained a hyperactive, mutated form of epidermal growth factor receptor, which triggered activation of downstream signaling pathways, such as mitogen-activated protein kinase and AKT, in cells that absorbed them.[12] Such a horizontal transfer mechanism can potentially deliver transforming signals of many kinds throughout tissues and even to distant sites.[12] Most TMVs described in the literature are in the approximately 80- to 500-nm-diameter range.[14–16] Because membrane blebbing can produce a type of microvesicle large enough to be detected by methods other than electron microscopy or biochemical isolation, the question we address herein is whether such a large tumor-derived vesicle can be observed and quantified *in situ* in tumor tissues or in the circulation. The Ras-like small GTP-binding protein ADP-ribosylation factor 6 (ARF6) was recently identified as a regulator of actomyosin-based abscission of protease-loaded vesicles from the plasma membrane of invasive tumor cell lines.[17] This mechanism results in secretion of relatively large, ARF6-enriched vesicles from blebbing cells,[17] suggesting the possibility that large oncosomes might be detected *in vivo* using antibodies to ARF6 or other informative target proteins.

In the present study, we used a series of prostate cancer models to test the hypothesis that large TMVs, termed large oncosomes herein, can be identified and quantified in plasma and tumor tissue. Our findings show that such structures may be a common feature of aggressive prostate cancer, including metastatic cancer in humans and mice; their evaluation can potentially provide information on disease aggressiveness; and their presence in the microenvironment could be functionally involved in metastatic dissemination and lethal biological behavior of human tumors.

Materials and Methods

Cell Culture

LNCaP, DU145, PC3, and WPMY-1 were from ATCC.[11,18,19] The LNCaP/LacZ and LNCaP/MyrAkt1 lines were described.[18] For the generation of LNCaP/Vo and LNCaP/caveolin-1 (Cav-1), parental LNCaP cells were plated at 70% to 80% confluence and transfected using Lipofectamine 2000 Tranfection Reagent (Invitrogen, Carlsbad, CA). Stable populations were isolated after selection with gentamicin G418, 0.5 mg/mL. The LNCaP cells were cultured in RPMI 1640 medium supplemented with 10% fetal bovine serum (Valley Biomedical, Winchester, VA), 2 mmol/L L-glutamine, 100 U/mL penicillin, and 100 μg/mL streptomycin (all from Invitrogen). The DU145 and PC3 cells were cultured in Dulbecco's modified Eagle's medium supplemented with 10% and 5% (WPMY-1) fetal bovine serum, 2 mmol/L L-glutamine, 100 U/mL penicillin, and 100 μg/mL streptomycin.

DNA and RNA Extraction

Total nucleic acid was isolated by the TRIzol (Invitrogen) extraction method, and concentration was determined by using the NanoDrop 2000c spectrophotometer (ThermoFisher Scientific, Inc., Waltham, MA). RNA and DNA were fractionated by gel electrophoresis on a 2% agarose gel (Invitrogen), and nucleic acid purity was evaluated by RNase A (Invitrogen) and DNase 1 (Sigma, St. Louis, MO) digestion. Nucleic acid (100 ng) from vesicles obtained from 2×10^7 LNCaP/MyrAkt1 cells was suspended in 15 μL of buffer for gel electrophoresis.

Immunoblot Analysis

Cells and purified vesicles were lysed and analyzed by SDS-PAGE and Western blot analysis with the following antibodies: rabbit polyclonal Cav-1 (N-20) (Santa Cruz Biotechnology, Santa Cruz, CA); HA.11 monoclonal antibody (mAb), clone 16B12 (Covance, Princeton, NJ); Akt1 and *p*-Akt1 (S473), clone D9E (Cell Signaling, Danvers, MA), at a dilution of 1:1000; and β-actin mAb, clone AC-15 (Sigma), at a dilution of 1:5000. The ARF6 antibody was a generous gift from Dr. Victor Hsu,

Brigham and Women's Hospital, Boston, MA.[11,20] Protein, 15 μg per lane, was loaded for Western blot analysis.

Immunofluorescence Microscopy

Cells were incubated on ice with fluorescein isothiocyanate (FITC)–conjugated cholera toxin B (CTxB) subunit (Sigma) or Alexa 594–conjugated CTxB (Invitrogen) and analyzed as previously described.[19] For selected experiments, LNCaP/MyrAkt1 cells were fixed in 4% paraformaldehyde, stained with FITC-conjugated HA (MyrAkt1) tag (Santa Cruz Biotechnology), and imaged using an Axioplan 2 microscope (Zeiss, Oberkochen, Germany).[19]

Animal Models and Tumor Xenografts

All experiments were performed in compliance with the guidelines of the Institutional Animal Care and Use Committee, Children's Hospital Boston (Boston). We established s.c. xenografts, injecting 2×10^6 LNCaP/LacZ or LNCaP/MyrAkt1 cells into the flanks of 8 and 16 mice with severe combined immunodeficiency, respectively. Tumor growth was monitored three times per week from the detection of the first palpable tumors, and the mice were sacrificed before reaching the maximum tumor burden of 2000 cm^3 at all four sites (6 weeks after implantation). At necropsy, tumors were removed, weighed, fixed in 10% buffered formalin, and embedded in paraffin for histological analysis. The colonies of transgenic mice with autochthonous prostate tumors (TRAMP) and age-matched wild-type mice were maintained in a C57BL6/J background and genotyped as previously described.[21,22] In some experiments, TRAMP mice from an F_1 C57BL6/J × FVB/N cross were used. $Pten^{PbKO}/Trp53^{PbKO}$ and $Pten^{PbKO}$/KRAS mice were maintained as previously described.[21]

Oncosome Isolation

Oncosomes were purified from conditioned medium or from 500 μL of platelet-poor plasma, as previously described.[11] Briefly, cells and debris were eliminated by centrifugation at 2800 × *g* for 10 minutes. The supernatant was centrifuged at 100,000 × *g* for 80 minutes. Purified oncosomes were washed in PBS, stained with the indicated antibodies, fixed and permeabilized in ethanol, then analyzed by fluorescence-activated cell sorting (FACS) and sorted using 1- and 10-μm bead standards, followed by microscopic examination. In selected experiments, unfixed large oncosomes were sorted using size gates with 1- and 10-μm bead standards and used for biological experiments.

Gelatin Zymography and in Vitro Degradation Assay

Lysed particles isolated from growth media were analyzed by gelatin zymography (substrate gel electrophoresis).[23] The gelatin degradation assay was performed by seeding isolated particles (1 to 5 μg) on FITC-labeled gelatin-coated coverslips for 1.5 hours, at 37°C, using a modification of a published protocol.[24]

Migration Assays

Mouse dermal endothelial cells (MDECs; 1×10^5), tumor endothelial cells (TECs), or DU145 cells treated with vesicles shed from cells (10 μg/mL) were stained with CellTracker RED CMPTX (Invitrogen), and assayed in Transwell FluoroBlok inserts for 16 hours. Cell migration was measured as previously described.[25] Alternatively, WPMY-1 cells (1.5×10^5) were seeded into the bottom of 24-well plates and treated for 24 hours with 10 μg/mL LNCaP/MyrAkt1 vesicles. DU145 cells (1×10^5), labeled with CellTracker, were seeded into FluoroBlok inserts placed into the WPMY-1–conditioned media and migration monitored, as previously described. Vesicles were unfixed when used in migration assays. Results represent fold changes from the average of biological triplicates performed in technical duplicate.

Flow Cytometry

Purified vesicles were stained with propidium iodide (PI) staining buffer (BD Bioscience, San Jose, CA) or with the indicated antibodies, processed on a Moflo High-Speed Cell Sorter (Beckman-Coulter, Brea, CA), and analyzed using FlowJo software (Treestar, Ashland, OR). Bead standards, 1 and 10 μm (Spherotech, Lake Forest, IL), were used to set size gates. At least 3000 events were recorded.[26] The following antibodies were used: HA-probe (F-7) FITC (Santa Cruz Biotechnology), at a dilution of 1:200, and Cav-1 (N-20) (Santa Cruz Biotechnology), at a dilution of 1:200.

Electron Microscopy

Large Oncosomes

Purified material was adsorbed to glow-discharged, carbon-coated copper grids and stained with 0.75% (w/v) uranyl formate, as previously described.[27] Images were collected on a Philips CM10 electron microscope (FEI, Hillsboro, OR) operated at an acceleration voltage of 100 kV. Images were recorded on a 1K charge-coupled device camera (Gatan, Pleasanton, CA) at a magnification of ×50,000 and a defocus of approximately −1.5 μm.

Human Xenografts

Sections from the paraffin-embedded s.c. tumors were deparaffinized and fixed for 2 hours in Karnovsky fixative before post-fixation with 1% OsO_4 and 0.03 g/4 mL of potassium ferrocyanide. Sections were then stained overnight with 2% uranyl acetate, dehydrated, and embedded overnight with a 1:1 mixture of LX 112 resin and 100% ethanol (Ladd Research, Williston, VT). Electron micrographs were collected on a JEOL 1400 TEM operated at an acceleration voltage of 120 kV.

Immunohistochemistry

Sections from the paraffin-embedded mice tumors, human core biopsy specimens, and human TMA were stained[18,19,28] with the following antibodies: Akt mAb (Cell Signaling) at a dilution of 1:500; HA.11 mAb, clone 16B12 (Covance), at a dilution of 1:100; and CK18 rabbit polyclonal Ab (Epitomics, Burlingame, CA), at dilution of 1:200. The ARF6 antibody was a generous gift from Dr. Victor Hsu.

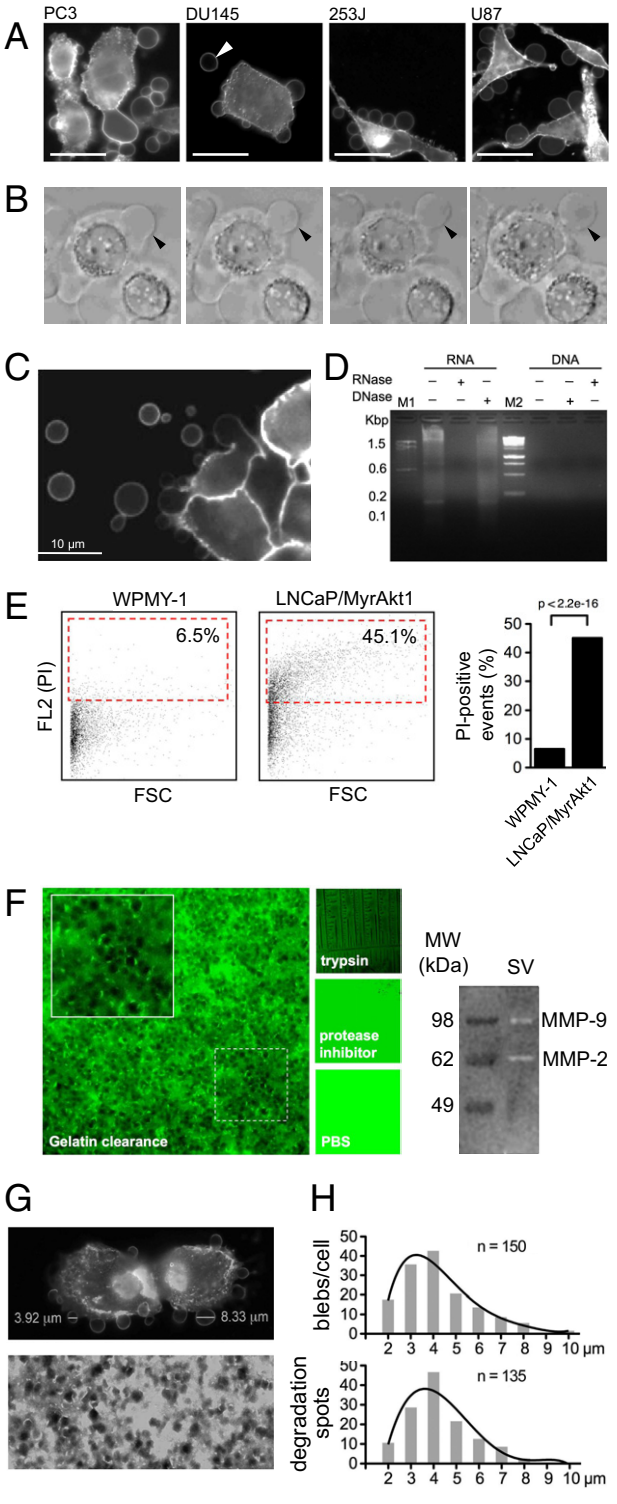

Patients and Samples

Three human tissue cohorts were used: i) core biopsy specimens with localized prostate cancer from 15 patients from the Department of Pathology, University of Naples, Naples, Italy; ii) a TMA from Ulm, Germany, containing 26 multifocal specimens, with at least two distinct cancer foci in the prostate gland and one lymph node metastasis; and iii) a TMA containing 36 benign prostate samples, 36 organ-confined tumors, and 36 metastatic tumors, of which 11, 20, and 23 samples, respectively, were available for the analysis.[19,29–31] Informed consent was obtained from all subjects.

Statistical Analysis

Comparisons between experimental groups were performed using a two-tailed, unpaired, Student's *t*-test. A Pearson's χ^2 test was used to assess the correlation between percentage of MyrAkt1-positive events and tumor weight. A Fisher's exact test was applied to assess the association between the presence of large oncosome-like structures and Gleason score groups and metastases. In all experiments, $P < 0.05$ was considered significant.

Results

Tumor cells that exhibited the amoeboid feature of membrane blebbing could release large, plasma membrane–derived vesicles into the extracellular space[11] (Figure 1, A and B, and Figure 2A). To determine whether these vesicles could be isolated and analyzed, we purified shed vesicles from the conditioned medium of LNCaP human prostate cancer cells stably expressing the potent oncogene MyrAkt1[18] and from WPMY-1 prostate stromal cells. The contents of the purified vesicles reacted with PI

Figure 1. Characterization and detection of shed tumor cell–derived vesicles. **A:** Prostate cancer (PC3 and DU145), bladder cancer (253J), and glioblastoma (U87) cell lines are stained with CTxB and imaged by confocal microscopy. Scale bar = 10 μm. **Arrowhead** denotes a large vesicle released in the extracellular space. **B:** CTxB-labeled DU145 cells showing large, bulbous membrane protrusions and several large vesicles released into the surrounding environment. **Arrowhead** points to a large membrane bleb resulting in a released vesicle. **C:** Nucleic acid extracted from vesicles shed from LNCaP/MyrAkt1 cells. Total RNA/DNA is treated with RNase A or DNase 1 and samples electrophoresed through 2% agarose (**D**). **E:** FACS analysis of vesicles, isolated from the medium of WPMY-1 and LNCaP/MyrAkt1 cells treated with epidermal growth factor (50 ng/mL), fixed, permeabilized, and stained with PI. The dot plots depict forward scatter signal (FSC) and FL2 (PI). The red gates surround PI-positive events, graphed on the right. $P < 2.2e\text{-}16$. **F: Left panel**, photomicrograph of FITC-labeled gelatin matrix loaded with a biochemical preparation of vesicles shed from LNCaP/MyrAkt1 cells, showing large zones of proteolytic clearance. Original magnification, ×40. Trypsin is used as a positive control; a general protease inhibitor and vehicle serve as negative controls. **Right panel**, shed vesicles (SVs) are analyzed via gelatin zymography (substrate gel electrophoresis), showing active MMP9 and MMP2. **G: Top panel**, LNCaP/MyrAkt1 cells are stained with FITC-CTxB. Two membrane vesicles are large. **Bottom panel**, FITC-labeled gelatin after exposure to SVs. The CTxB-labeled membrane blebs ($n = 150$; **G**) and gelatin degradation spots ($n = 135$; **H**) are measured by AxioVision version 4.5 (Zeiss) and plotted graphically (mode, 3.1 to 4 μm).

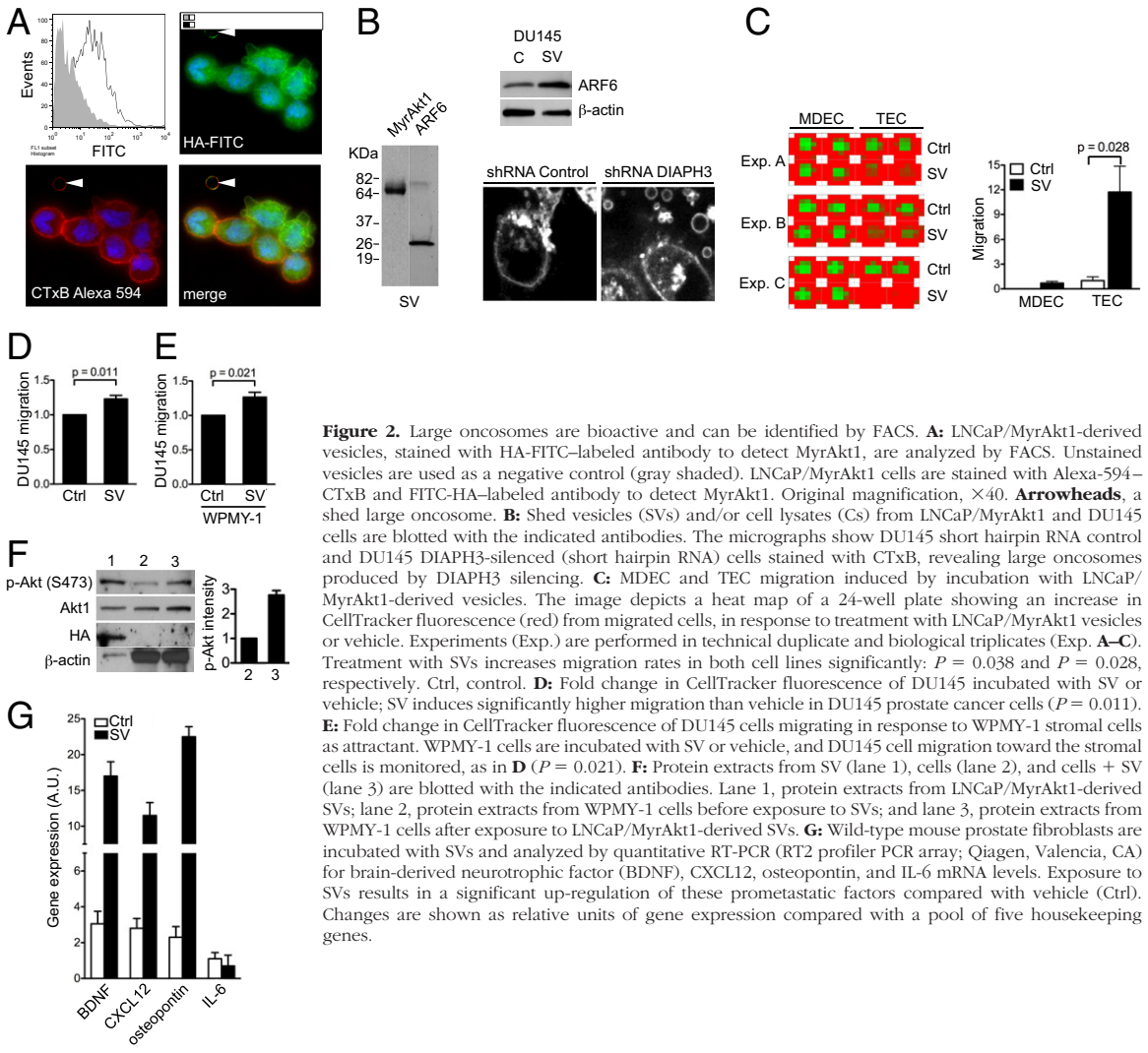

Figure 2. Large oncosomes are bioactive and can be identified by FACS. **A:** LNCaP/MyrAkt1-derived vesicles, stained with HA-FITC–labeled antibody to detect MyrAkt1, are analyzed by FACS. Unstained vesicles are used as a negative control (gray shaded). LNCaP/MyrAkt1 cells are stained with Alexa-594–CTxB and FITC-HA–labeled antibody to detect MyrAkt1. Original magnification, ×40. **Arrowheads**, a shed large oncosome. **B:** Shed vesicles (SVs) and/or cell lysates (Cs) from LNCaP/MyrAkt1 and DU145 cells are blotted with the indicated antibodies. The micrographs show DU145 short hairpin RNA control and DU145 DIAPH3-silenced (short hairpin RNA) cells stained with CTxB, revealing large oncosomes produced by DIAPH3 silencing. **C:** MDEC and TEC migration induced by incubation with LNCaP/MyrAkt1-derived vesicles. The image depicts a heat map of a 24-well plate showing an increase in CellTracker fluorescence (red) from migrated cells, in response to treatment with LNCaP/MyrAkt1 vesicles or vehicle. Experiments (Exp.) are performed in technical duplicate and biological triplicates (Exp. **A–C**). Treatment with SVs increases migration rates in both cell lines significantly: $P = 0.038$ and $P = 0.028$, respectively. Ctrl, control. **D:** Fold change in CellTracker fluorescence of DU145 incubated with SV or vehicle; SV induces significantly higher migration than vehicle in DU145 prostate cancer cells ($P = 0.011$). **E:** Fold change in CellTracker fluorescence of DU145 cells migrating in response to WPMY-1 stromal cells as attractant. WPMY-1 cells are incubated with SV or vehicle, and DU145 cell migration toward the stromal cells is monitored, as in **D** ($P = 0.021$). **F:** Protein extracts from SV (lane 1), cells (lane 2), and cells + SV (lane 3) are blotted with the indicated antibodies. Lane 1, protein extracts from LNCaP/MyrAkt1-derived SVs; lane 2, protein extracts from WPMY-1 cells before exposure to SVs; and lane 3, protein extracts from WPMY-1 cells after exposure to LNCaP/MyrAkt1-derived SVs. **G:** Wild-type mouse prostate fibroblasts are incubated with SVs and analyzed by quantitative RT-PCR (RT2 profiler PCR array; Qiagen, Valencia, CA) for brain-derived neurotrophic factor (BDNF), CXCL12, osteopontin, and IL-6 mRNA levels. Exposure to SVs results in a significant up-regulation of these prometastatic factors compared with vehicle (Ctrl). Changes are shown as relative units of gene expression compared with a pool of five housekeeping genes.

(see Supplemental Figure S1A at *http://ajp.amjpathol.org*), consistent with the presence of RNA (Figure 1C). This allowed us to detect a PI-positive vesicle population by FACS. The stromal cells produced substantially fewer vesicles than the LNCaP/MyrAkt1 cells ($P < 0.001$) (Figure 1D). Thus, biochemical purification, coupled with FACS, was in agreement with results using a visual quantitative bleb formation assay.[11] Shed vesicles from LNCaP/MyrAkt1 cells produced zones of proteolytic clearance in a fluorescent gelatin matrix assay[24] (Figure 1E) in a similar size range (2 to 4 μm) and modal distribution to >1-μm-diameter membrane blebs observed microscopically (Figure 1, F and G). Matrix metalloproteinase (MMP) zymography showed that the vesicle preparations contained bioactive MMP9 and MMP2, two key proteases involved in tumor cell invasion (Figure 1E).

Shed vesicles isolated from LNCaP/MyrAkt1 cells contained abundant, membrane-localized MyrAkt1, as demonstrated by FACS and immunofluorescence staining (Figure 2A) and by Western blot analysis (Figure 2B). These results indicated that MyrAkt1 is a potentially useful marker with which to track large shed vesicles produced by LNCaP/MyrAkt1 cells *in vivo*. Vesicles shed and purified from U87 glioma cells, which exhibited amoeboid properties, contained Cav-1, similar to DU145 prostate cancer cell–derived vesicles.[11] DU145 and LNCaP/MyrAkt1 vesicle preparations also contained ARF6 (Figure 2B), a GTPase recently shown to mediate large microvesicle shedding from tumor cells[17] and to be enriched in TMV.[17] As previously reported,[11] silencing of the GTPase-regulated formin DIAPH3 in DU145 cells potentiated shedding of large microvesicles (Figure 2B). As reported in another recent study, DIAPH3 loss in DU145 and other tumor cell backgrounds resulted in amoeboid behavior,[10] providing further evidence that shedding of large TMVs were a feature of the amoeboid tumor phenotype.

Sustained ARF6 activation has enhanced tumor cell invasion in cell and animal model systems,[32,33] and vesicle shedding may be a potential mechanism for ARF6-induced acquisition of invasive potential.[17] Interrogation of publicly available prostate cancer expression data sets demonstrated that ARF6 mRNA levels were higher in prostate cancer compared with benign tissue (see Sup-

plemental Figure S1 at *http://ajp.amjpathol.org*).[34–38] Significantly, ARF6 ranked in the top 10 percentile of overexpressed genes in these data sets, and ARF6 mRNA was significantly up-regulated in metastases and in recurrent disease.

The MMP activity seen with large vesicles shed from LNCaP/MyrAkt1 cells (Figure 1, F–H) indicated that they were bioactive. In separate bioactivity tests, these vesicle preparations stimulated migration of mouse TECs, MDECs[39] (Figure 2C), and DU145 cells (Figure 2D). LNCaP/MyrAkt1 vesicles also activated WPMY-1 stromal cells to produce factors that stimulated migration of DU145 cells (Figure 2E). LNCaP/MyrAkt1 vesicles also activated Akt1 in WPMY-1 stromal cells (Figure 2F). Finally, incubation of mouse prostatic fibroblastic cells with LNCaP/MyrAkt1 vesicles resulted in increased expression of prometastatic factors: brain-derived neurotrophic factor, CXCL12, and osteopontin[40–42] (Figure 2G). Collectively, these data indicated that LNCaP/MyrAkt1 cells shed oncosomes, including particles considerably larger than nanosized microvesicles, with the potential to contribute to oncogenic signaling by acting as paracrine effectors of intertumor cell, tumor-endothelial cell, and epithelial-stromal reaction.

Large Oncosomes in the Circulation and in Situ

To distinguish large oncosomes from smaller TMV unequivocally, we used ultracentrifugation and immuno–flow cytometry in combination with sizing beads to generate a calibrated domain of analysis based on size. After biochemical purification, shed vesicles were stained with DAPI to verify the absence of cellular contamination (see Supplemental Figure S2A at *http://ajp.amjpathol.org*) and subsequently labeled with an HA antibody for detection of membrane-localized MyrAkt1.[18] MyrAkt1-negative and MyrAkt1-positive populations were then distinguished on a cell sorter, with gates set using 1- and 10-μm beads (Figure 3A; see also Supplemental Figure S2B at *http://ajp.amjpathol.org*). Because aggregates might potentially be a significant component of the vesicle preparation, we excluded them from the analysis. To do this, a forward scatter signal was plotted against pulse width (PW) of the same signal on a linear scale (Figure 3A). Electronic signal pulses were composed of pulse height and PW, and the latter was a function of the time necessary to traverse the laser beam, which was shorter for single particles. Electric pulses from a flow cytometer detector with a narrow PW identified a singlet (bottom), whereas those with a broader PW identified doublets or possibly clumps (top). To restrict our analysis to single vesicles, we delineated a region in which only single events were analyzed based on their smaller and more homogeneous PW signals and their corresponding forward scatter signals[26] (Figure 3A). Only these events were gated and considered for further analysis (Figure 3A). Electric pulses generated from aggregates, as indicated by increased PW (Figure 3A), were excluded from the analysis,[26] as validated microscopically (Figure 3, A and B). Sorted single events (≤1 and >1 μm) were visualized by both fluorescence and electron microscopy, indicating that large, single vesicles could be distinguished within a mixed population. Microscopic analysis of retrieved vesicles after ultracentrifugation and other sorting procedures indicated that they were not aggregates of smaller particles and that they had a definable structure (Figure 3, A and B). These results indicated that large vesicles could be isolated as discrete events using a tumor cell–specific marker.

After having demonstrated that membrane blebs shed by cells could be sorted by FACS as discrete large vesicles, we attempted to use a similar approach to isolate and quantify these blebs in the circulation of mice with severe combined immunodeficiency carrying LNCaP/MyrAkt1 xenograft tumors. All mice injected s.c. with either LNCaP/MyrAkt1 or LNCaP/LacZ control cells in Matrigel developed tumors; however, LNCaP/MyrAkt1 tumors were significantly larger than LNCaP/LacZ tumors (Figure 4A; see also Supplemental Figure S3A at *http://ajp.amjpathol.org*). Akt1 was membrane localized in LNCaP/MyrAkt1 tumors, as detected with both Akt1 and HA antibodies (Figure 4B; see also Supplemental Figure S3C at *http://ajp.amjpathol.org*), confirming *in vitro* findings.[18] The HA antibody was highly specific and did not recognize antigens in LNCaP/LacZ tumors (see Supplemental Figure S3C at *http://ajp.amjpathol.org*). Plasma

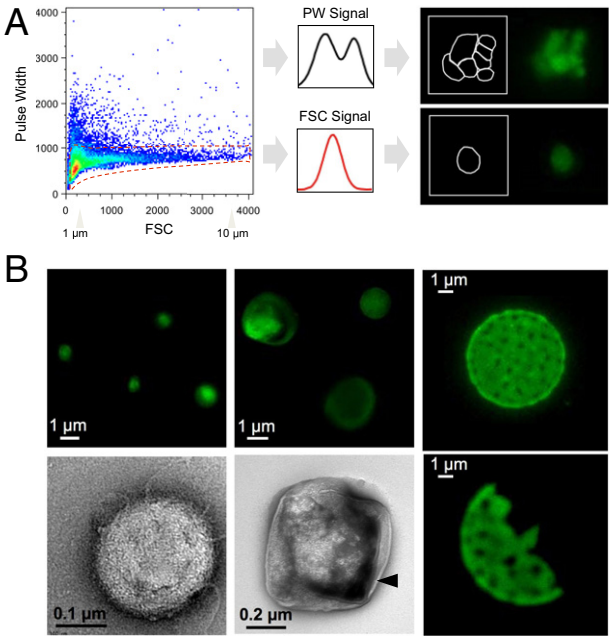

Figure 3. Analysis of shed vesicles and detection of large oncosomes by FACS and microscopy. **A:** Purified vesicles are derived from LNCaP/MyrAkt1 cells, stained with an FITC-conjugated HA antibody, and plotted by setting a forward scatter signal (FSC) versus a PW signal on a linear scale (**left panel**). **Right panels**, a schematic representation of two signal pulses from the flow cytometer detector, corresponding to single particles (**bottom panel**) and doublet particles (**top panel**). Gated single events (within the red dotted line on the **left panel**) are visualized at the microscope and considered for further analysis. Signal pulses generated from aggregates (outside of the red dotted line) are excluded. **B:** Fluorescence and electron micrographs of MyrAkt1-positive particles sorted using size beads ≤1 and >1 μm. **Arrowhead**, lipid bilayer structure of the vesicle-encapsulating membrane.

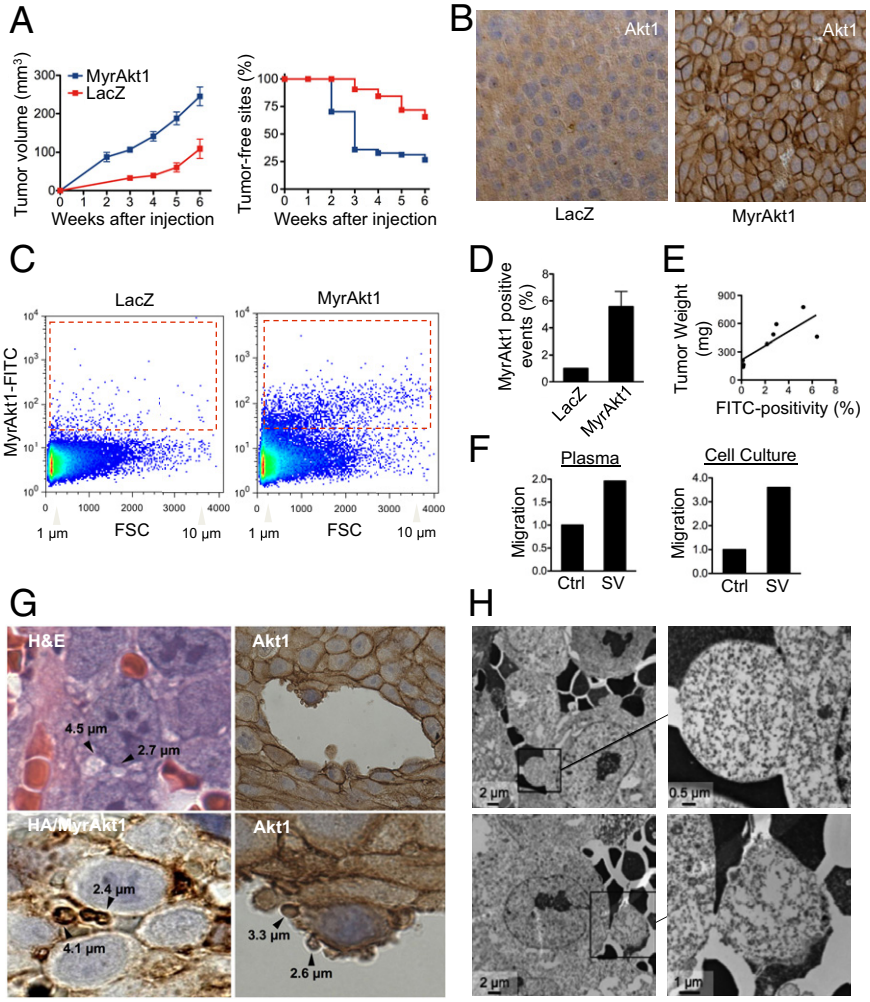

Figure 4. Identification of large oncosomes *in vivo*. **A:** Tumor growth and tumor take in LNCaP/MyrAkt1 and LNCaP/LacZ xenografts (growth, $P < 0.01$; s.c. sites free of tumor, $P = 0.01$). **B:** Akt1 immunostaining of paraffin sections of the indicated xenografts. There is prominent Akt membrane staining in the MyrAkt1 tumors, in contrast to its diffuse cytosolic staining in the LacZ tumor sections. **C: Left panel**, FACS analysis of 1- to 10-μm MyrAkt1-positive vesicles purified from the plasma of mice carrying LNCaP/MyrAkt1 and LNCaP/LacZ xenografts. Dot plot, forward scatter signal (FSC) and FL1 (MyrAkt1); red gate, positive events. **D:** Quantitative evaluation of MyrAkt1-positive events. A cutoff corresponding to the 99th percentile of vesicles isolated from the plasma of mice with LNCaP/LacZ tumors is chosen to segregate negative and positive events. **E:** In mice with LNCaP/MyrAkt1 tumors, the percentage of MyrAkt1-positive vesicles correlates with tumor weight. $^{*}P = 0.007$. **F:** MDECs exhibit increased migration when exposed to oncosomes compared with vehicle. **Left panel**, the vesicles are isolated from the plasma of mice with MyrAkt1 tumors. **Right panel**, the vesicles are derived from the medium of LNCaP/MyrAkt1 cells. Ctrl, control; SV, shed vesicle. **G:** Tumor sections of LNCaP/MyrAkt1 xenografts are stained with H&E. **Arrowheads**, large vesicles, similar in appearance to large oncosomes. Sections are also immunostained with an Akt1 antibody, which identifies Akt1 at the plasma membrane and allows visualization of large vesicles. **H:** Tumor sections of LNCaP/MyrAkt1 xenografts are imaged by transmission electron microscopy. Membrane blebs protruding from tumor cells near blood vessels are highlighted.

from mice carrying LNCaP/MyrAkt1 tumors contained MyrAkt1-positive events in the 1- to 10-μm range that were sorted with the HA antibody (Figure 4, C and D). The number of MyrAkt1 events detected by FACS correlated with tumor weight ($P < 0.01$) (Figure 4E). Because the HA antibody did not recognize an endogenous epitope in the mouse,[18] these data indicated that tumor-derived large vesicles from the s.c. xenografts gained access to the circulation.

Strikingly, MyrAkt1-positive vesicles isolated from the blood of mice with MyrAkt1 tumors stimulated migration of normal endothelial cells (Figure 4F), suggesting the capability of oncosomes in the circulation to evoke progression-related changes in the microvasculature. A similar result was obtained with MyrAkt1-positive vesicles sorted by FACS in the 1- to 10-μm range from the medium of LNCaP/MyrAkt1 cells (Figure 4F), indicating that large oncosomes were bioactive.

High-magnification microscopy of LNCaP/MyrAkt1 tumors revealed membrane vesicles within a similar size range to the large oncosomes identified *in vitro* and in the circulation of the same animals (Figure 4G). To our knowledge, this type of membrane vesicle has not been previously described in paraffin sections of prostate tumors. Large oncosome-like structures were evident when sections of LNCaP/MyrAkt1 tumors were stained with H&E and immunostained with Akt1 and HA antibodies (Figure 4G; see also Supplemental Figure S3D at *http://ajp.amjpathol.org*). Morphological features with the appearance of intravasating amoeboid cells were identifiable by immunostaining with Akt1 antibody (Figure 4G). Akt1-positive vesicles in tumor tissues were also positive for ARF6 (see Supplemental Figure S3D at *http://ajp.amjpathol.org*), thus resembling large oncosomes secreted from LNCaP/MyrAkt1 and DU145 cells (Figure 2B), and in accordance with the amoeboid character of these cell lines.[11] Transmission electron microscopy of LNCaP/MyrAkt1 tumor sections showed that the tumor cells produced large, bulbous structures with the appearance of membrane sacs,[43] often in the proximity of vascular lacunae (Figure 4H; see also Supplemental Figure S3E at *http://ajp.amjpathol.org*). A higher magnification revealed internal structures with features resembling polyribosomes (see Supplemental Figure S3F at *http://ajp.amjpathol.org*). These results suggested that MyrAkt1-positive vesicles detected in the circulation of tumor-bearing mice arose from membrane blebs similar or identical to amoeboid blebs produced in cell culture.

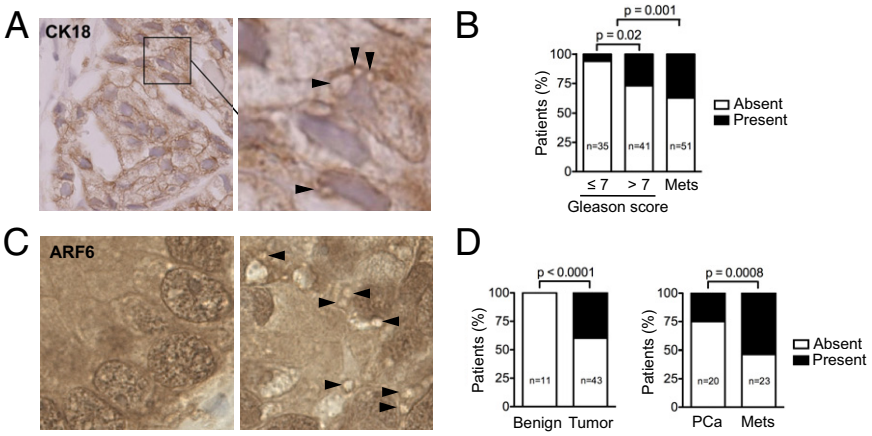

Figure 5. Large oncosome-like vesicles in metastatic prostate cancer. **A:** Representative paraffin section of human core biopsy specimens of patients with prostate cancer (Gleason score, 4 + 3) are immunostained with CK18 antibody. **Arrowheads**, structures resembling large oncosomes. **B:** Quantitative analysis of the distribution of ARF6-positive large oncosome-like vesicles among the diagnostic categories, showing vesicles are significantly more abundant in those with a Gleason score of >7 than a Gleason score of ≤7 ($P = 0.020$) and in metastases (Mets) than in organ-confined tumors [prostate cancer (PCa)] ($P = 0.001$). **C:** Representative sections of an additional prostate cancer TMA stained with ARF6, showing the absence (**left panel**) and presence (**right panel**) of large oncosome-like vesicles (**arrowheads**). **D:** The presence of structures resembling large oncosomes significantly discriminates between normal and tumor samples ($P < 0.0001$) and between organ-confined disease and metastasis ($P = 0.0008$).

Large Oncosome-Like Vesicles as a Feature of Metastatic Prostate Cancer

Next, we investigated whether similar large vesicles could be identified in human prostate cancer specimens. ARF6 staining revealed vesicular structures in the 1- to 10-μm range. We initially examined a small cohort of human core biopsy specimens ($n = 15$) with localized prostate cancer, and identified ARF6-positive large oncosome-like structures in the tumor tissue of three specimens (see Supplemental Figure S4A at *http://ajp.amjpathol.org*). Significantly, similar vesicular structures were also identified using a CK18 antibody, which detected prostate luminal epithelial cells (Figure 5A). To determine whether the identification of ARF6-positive vesicles in tissues might reflect clinical status, we examined a TMA[44] containing >120 punches from foci of localized and metastatic human prostate cancer. High magnification revealed ARF6-positive vesicles more frequently in foci with a Gleason score >7 compared with foci with a lower Gleason score ($P = 0.02$), suggesting that identification of large oncosome-like structures *in situ* might indicate tumor progression (see Supplemental Figure S4B at *http://ajp.amjpathol.org*). Notably, metastatic foci exhibited significantly more vesicles ($P = 0.001$) (Figure 5B). These characteristics represented a previously unrecognized histological feature of aggressive prostate cancer.

To determine whether the presence of vesicular structures identified using similar criteria could differentiate indolent versus fatal cancer, we used two models of *Pten*-deficient mice with a greatly different biological course. $Pten^{PbKO}/Trp53^{PBKO}$ mice developed prostate adenocarcinoma that remained organ confined within 10 to 16 weeks after gestation. In comparison, $Pten^{PbKO}/KRAS$ mice developed distant metastases in the liver and lung, and they also developed castrate resistance after androgen ablation.[21,22] ARF6-positive vesicles, similar in appearance and size to those seen in the LNCaP/MyrAkt1 tumors, were abundant in $Pten^{PbKO}/KRAS$ tissues but were absent in the $Pten^{PbKO}/Trp53^{PbKO}$ prostatic tissues (see Supplemental Figure S4C at *http://ajp.amjpathol.org*). These findings suggested that large oncosome features in prostate tumors might generally report aggressive disease.

We interrogated an additional human prostate TMA containing benign samples, organ-confined tumors, and metastatic tumors.[19,28,29] Figure 5C shows representative images of the absence and presence of large oncosome-like structures detected using anti-ARF6. These features were present in <30% of the tumors and were not detected in benign prostate tissue. We observed a significant correlation between the presence of large oncosome-like features and metastasis ($P = 0.0008$). The presence of these features also discriminated between benign and tumor tissue ($P < 0.0001$) (Figure 5D).

Large Oncosomes Containing Cav-1 Identify Aggressive Prostate Cancer

To determine whether large oncosomes could be identified using an endogenous tumor progression marker, we attempted to sort large shed vesicles using Cav-1, a validated prostate cancer biomarker found in the circulation of patients with advanced disease.[45] Cav-1 was present in membrane vesicles produced by DU145 cells, suggesting that large shed vesicles were a mobile vehicle for circulating Cav-1 (Figure 2B).[11] Cav-1–null LNCaP cells stably expressing Cav-1–green fluorescent protein (GFP) produced membrane vesicles that were shed and contained the fluorescent GFP fusion protein (see Supplemental Figure S5, A–C, at *http://ajp.amjpathol.org*). Enforced expression of Cav-1 in LNCaP cells significantly increased the rate of membrane blebbing and shedding (see Supplemental Figure S5D at *http://ajp.amjpathol.org*), suggesting that Cav-1 might play an active role in vesiculation. The ability to sort Cav-1–GFP–positive particles by FACS (data not shown) in the 1- to 10-μm range was validated with a Cav-1–Cy3 antibody, which decorated large oncosome-like GFP-positive vesicles (see Supplemental Figure S6A at *http://ajp.amjpathol.org*). By using the same approach, we detected endogenous Cav-1 in shed vesicle preparations from DU145 cells (see Supplemental Figure S6B at *http://ajp.amjpathol.org*). These results sug-

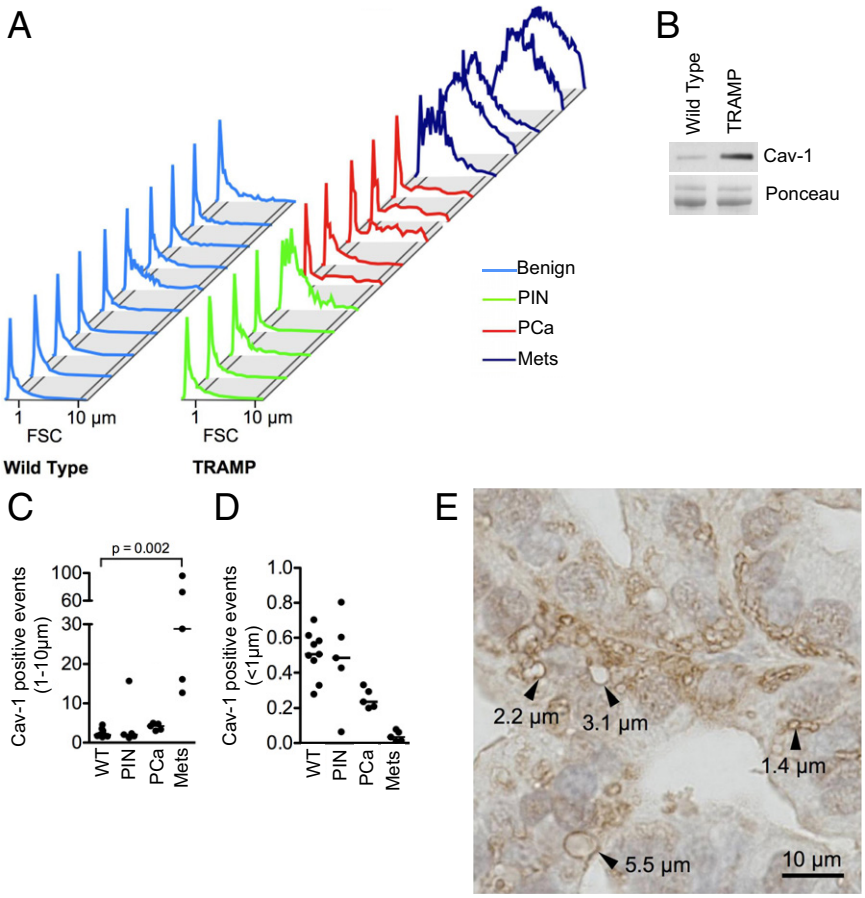

Figure 6. Large oncosome-like structures containing Cav-1 identify aggressive prostate cancer. **A:** FACS analysis of 1- to 10-μm Cav-1–positive vesicles are purified from the plasma of TRAMP (n = 15) and non-transgenic littermates (WT) (n = 10), plotted in a forward scatter signal (FSC) histogram, and analyzed with respect to the diagnostic categories. Mets, metastases; PCa, prostate cancer; PIN, prostate intraepithelial neoplasia. **B:** Large oncosome-like structures, isolated from the plasma of TRAMP and WT mice, are analyzed by Western blot analysis. **C:** The abundance of Cav-1–positive large oncosome-like structures (1 to 10 μm) is significantly increased in tumor-bearing mice than in controls (P = 0.0007), and dramatically correlates with disease progression (almost 30-fold difference between mice with organ-confined tumors and mice with lung metastases) (P = 0.0002). **D:** The abundance of Cav-1–positive events <1 μm does not reflect changes across the diagnostic categories. **E:** Representative paraffin section of a TRAMP metastatic tumor is stained with ARF6 antibody. **Arrowheads,** large oncosome-like structures.

gested that Cav-1 was a viable target for identifying large oncosomes.

We next attempted to sort Cav-1–positive vesicles from the plasma of transgenic mice with autochthonous prostate tumors (TRAMP). TRAMP prostate tissues expressed high levels of intratumoral Cav-1.[28,46] Age-matched, non-transgenic littermates were used as controls. We again focused our analysis on vesicles with a 1- to 10-μm diameter. As a validation method, Cav-1–positive vesicles (>2 to 3 μm) detected in plasma were sorted by FACS and visualized by direct optical imaging (see Supplemental Figure S7 at *http://ajp.amjpathol.org*). Vesicles meeting these criteria were detected in plasma from TRAMP mice with prostate cancer, but levels were negligible in plasma of non-transgenic animals and of TRAMP animals with prostate intraepithelial neoplasia (Figure 6A), as confirmed by Western blot analysis (Figure 6B). These vesicles were substantially more abundant in the circulation of TRAMP mice with lymph node and lung metastases (P = 0.03) (Figure 6, A and C; see also Supplemental Figure S8 at *http://ajp.amjpathol.org*). These results suggested that large oncosomes containing Cav-1 reached the circulation of mice with prostate cancer, and their presence could reflect the extent of disease progression. Notably, the presence of Cav-1–positive vesicles <1 μm, which were also detected in the plasma, was not correlated with disease progression in this model (Figure 6D). Significantly, large oncosome-like vesicles recognized using ARF6 staining were also identified *in situ* in metastatic TRAMP tumors (Figure 6E), whereas they were not detected in organ-confined tumors or in benign tissue.

Discussion

This study describes a type of bioactive membrane vesicle previously unrecognized *in vivo*, which can originate from amoeboid tumor cells. This class of microvesicle is large (approximately 1- to 10-μm diameter) compared with other types of bioactive vesicles (<1 μm), in particular the substantially smaller exosome-sized vesicles[47] (30 to 100 nm; see Supplemental Figure S9 at *http://ajp.amjpathol.org*). Consequently, we propose the term large oncosome as a descriptor. Whether biological and structural differences exist between these vesicles and other TMVs remains to be determined.

We show that prostate cancer cell–derived oncosomes exhibited proteolytic activity on gelatin, and contained bioactive MMP9 and MMP2, suggesting that they could be a means to focally concentrate proteases that facilitate migration of tumor cells, thus promoting metastasis. Accordingly, large oncosome-enriched preparations stimulated migration of DU145 cells, and the result was accentuated using medium conditioned by stromal cells exposed to oncosome material. Oncosomes and

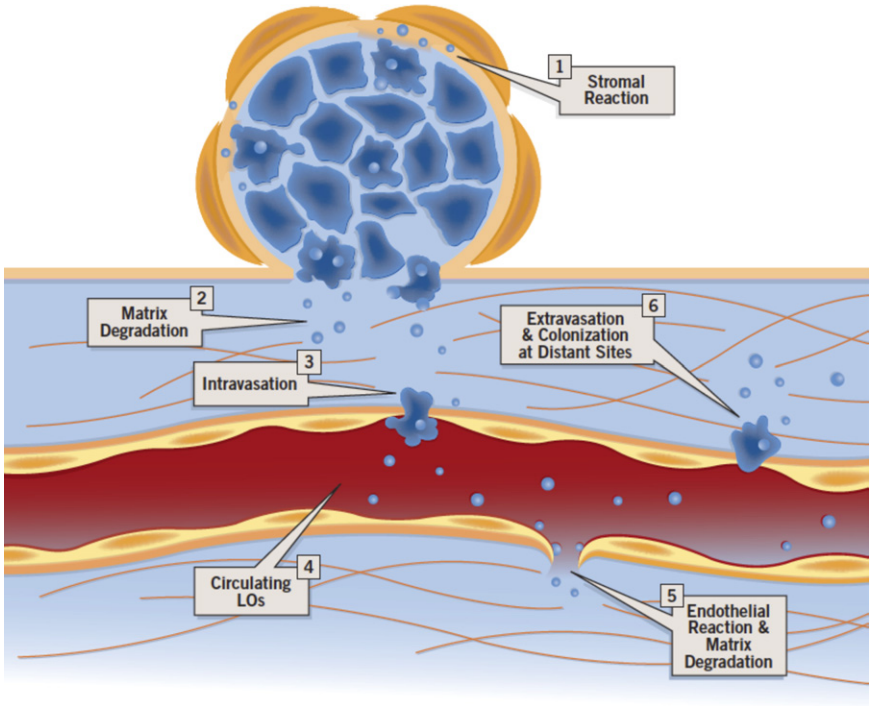

Figure 7. Model of potential sites of oncosome bioactivity. Our results suggest a working model in which oncosomes modify the microenvironment by inducing stromal reaction, ECM degradation, and migration of endothelial cells. Through these processes, circulating tumor-derived particles may promote endothelial leakage, allowing extravasation and colonization of distant sites. LO, large oncosome.

other TMVs are potential mediators of poorly understood phenomena, such as intravasation and extravasation, tumor dormancy, and preparation of distant sites before implantation of metastatic cells, as supported by several lines of functional evidence.[48] In support of this conclusion, our results show that large oncosome preparations stimulate migration of mouse TECs and, to a lesser extent, MDECs,[39] suggesting that these TMVs might disrupt the integrity of endothelial cell junctions and thereby increase blood vessel permeability *in vivo*. The fact that TECs exhibit a greater migratory response than normal endothelial cells suggests a putative mechanism underlying the greater permeability of tumor blood vessels. Oncosomes shed from tumor cells may condition the microenvironment in a manner that favors the production of soluble factors from stromal cells.[49] Through degradation of the ECM, they could release endothelial permeabilization factors that facilitate intravasation.[50] Oncosomes may also induce epigenetic changes and reprogram endothelial cells by transferring RNA, as has been hypothesized for other types of microvesicles.[48] Because oncosomes can also induce migration of normal endothelial cells, circulating tumor-derived oncosomes might promote endothelial leakage, allowing extravasation and colonization of distant sites (Figure 7).

Our study describes several independent approaches for the detection of large oncosomes in the circulation and in formalin-fixed, paraffin-embedded (FFPE) sections from mouse models and human tumors. Unlike smaller particles, we show that large oncosome-like structures are visible in tissues using conventional methods, including detection with a clinical biomarker (CK18; Figure 4D) in FFPE tissue sections, suggesting that a method for detecting these pathological features could be adapted for routine histopathological analysis. We also show that large oncosomes can be quantified in platelet-poor plasma. In several prostate cancer models, and in human TMAs and core biopsy specimens, large oncosome-like structures are a feature associated with high Gleason grade and metastatic disease. Our findings, particularly those using the LNCaP/MyrAkt1 model, in which the oncosomes can be followed from the point of secretion in tissues to circulation in the blood stream *in vivo*, support the conclusion that large oncosomes are produced by aggressive tumor cells and gain access to the circulation. In the present study, we focused on prostate cancer models. However, because similar processes occur in other solid tumors, we believe it is likely that similar particles may be detected in other malignancies using comparable approaches. Our analysis of the features of these large TMVs by microscopy indicates that they have an intrinsic structure, suggesting that they may be stable, possibly for long periods.

By using specific markers and an FACS method that allowed sorting of vesicles (1- to 10-μm diameter) and exclusion of aggregates, our results show a correlation between the abundance of large oncosomes in the plasma and tumor weight, in mice carrying LNCaP/MyrAkt1 xenograft tumors. In tissues, we detected large vesicles by direct inspection of H&E-stained tumor sections. ARF6 immunostaining facilitated the detection of similar structures in paraffin-embedded tissue, including in *Pten*^{PbKO}*/KRAS* metastatic prostate tumors, whereas they were not observed in organ-confined *Pten*^{PbKO} tumors. More important, *Pten*^{PbKO}*/KRAS* mice develop resistance to androgen ablation, suggesting that quantification of large oncosome-like features might facilitate assessment of tumor aggressiveness at initial presentation or disease progression during therapy. In TRAMP animals, the abundance of Cav-1–positive circulating

large oncosome-like structures was highly associated with the presence of metastatic tumors, and similar vesicular structures were observed in paraffin sections only from advanced tumors (Figure 6). Notably, the number of smaller events (<1 μm) in the circulation of TRAMP mice did not correlate with disease progression.

Our findings using independent cohorts of human prostate cancer tissues demonstrate that the large oncosome features discriminate between tumor and benign tissue, including benign prostatic hyperplasia, and also between organ-confined and metastatic tumors. Identifying predictive criteria for prostate tumor progression has been extremely problematic, and current paradigms, including prostate-specific antigen levels, Gleason score, and clinical stage, are inadequate as predictive tools. In particular, serum prostate-specific antigen can be elevated in benign conditions, such as inflammation and benign prostatic hyperplasia. Collectively, these observations indicate that assessment of large oncosome features in tumor sections or in the circulation might inform clinical evaluation. The identification of proteins other than Cav-1 and ARF6 in oncosomes, and discrete RNA species, might result in additional biomarker tools applicable to clinical medicine. Cav-1 is expressed by normal endothelial cells and has been identified as a constituent of circulating nanovesicles.[29] For this reason, it is possible that gating particle size >1 μm when Cav-1 is used as a sorting marker will provide information about disease course that collection of a smaller TMV may not.

Quantitation of circulating tumor cells (CTCs) is being evaluated to assess the risk of disease progression for prostate and other types of cancer. However, the clinical significance of CTCs remains to be established because of their extremely small number in peripheral blood compared with the number of blood cells.[51] We have demonstrated that large oncosome-like structures can be separated from plasma in a manner that does not require the capture of CTCs or other cells. The molecular characterization of large oncosomes may potentially offer a more sensitive and specific liquid biopsy than CTCs for patient selection, monitoring of treatment efficacy, and assessment of drug resistance.

Acknowledgments

We thank Drs. Thomas Walz and Susan Hagen for assistance with electron microscopy, Dr. Keith Solomon for helpful discussions, and Paul Guthrie and Kristine Pelton for technical assistance.

References

1. Yap TA, Zivi A, Omlin A, de Bono JS: The changing therapeutic landscape of castration-resistant prostate cancer. Nat Rev Clin Oncol 2011, 8:597–610
2. Yilmaz M, Christofori G, Lehembre F: Distinct mechanisms of tumor invasion and metastasis. Trends Mol Med 2007, 13:535–541
3. Kessenbrock K, Plaks V, Werb Z: Matrix metalloproteinases: regulators of the tumor microenvironment. Cell 2010, 141:52–67
4. Yilmaz M, Christofori G: Mechanisms of motility in metastasizing cells. Mol Cancer Res 2010, 8:629–642
5. Sanz-Moreno V, Gadea G, Ahn J, Paterson H, Marra P, Pinner S, Sahai E, Marshall CJ: Rac activation and inactivation control plasticity of tumor cell movement. Cell 2008, 135:510–523
6. Deakin NO, Turner CE: Distinct roles for paxillin and Hic-5 in regulating breast cancer cell morphology, invasion, and metastasis. Mol Biol Cell 2011, 22:327–341
7. Belgiovine C, Frapolli R, Bonezzi K, Chiodi I, Favero F, Mello-Grand M, Dei Tos AP, Giulotto E, Taraboletti G, D'Incalci M, Mondello C: Reduced expression of the ROCK inhibitor Rnd3 is associated with increased invasiveness and metastatic potential in mesenchymal tumor cells. PLoS One 2010, 5:e14154
8. Gadea G, de Toledo M, Anguille C, Roux P: Loss of p53 promotes RhoA-ROCK-dependent cell migration and invasion in 3D matrices. J Cell Biol 2007, 178:23–30
9. Maugis B, Brugues J, Nassoy P, Guillen N, Sens P, Amblard F: Dynamic instability of the intracellular pressure drives bleb-based motility. J Cell Sci 2010, 123:3884–3892
10. Hager MH, Morley S, Bielenberg DR, Gao S, Morello M, Holcomb IN, Liu W, Mouneimne G, Demichelis F, Kim J, Solomon KR, Adam RM, Isaacs WB, Higgs HN, Vessella RL, Di Vizio D, Freeman MR: DIAPH3 governs the cellular transition to the amoeboid tumour phenotype. EMBO Mol Med 2012, 4:743–760
11. Di Vizio D, Kim J, Hager MH, Morello M, Yang W, Lafargue CJ, True LD, Rubin MA, Adam RM, Beroukhim R, Demichelis F, Freeman MR: Oncosome formation in prostate cancer: association with a region of frequent chromosomal deletion in metastatic disease. Cancer Res 2009, 69:5601–5609
12. Al-Nedawi K, Meehan B, Micallef J, Lhotak V, May L, Guha A, Rak J: Intercellular transfer of the oncogenic receptor EGFRvIII by microvesicles derived from tumour cells. Nat Cell Biol 2008, 10:619–624
13. Lee TH, D'Asti E, Magnus N, Al-Nedawi K, Meehan B, Rak J: Microvesicles as mediators of intercellular communication in cancer: the emerging science of cellular "debris".Semin Immunopathol 2011, 33:455–467
14. Cocucci E, Racchetti G, Meldolesi J: Shedding microvesicles: artefacts no more. Trends Cell Biol 2009, 19:43–51
15. Al-Nedawi K, Meehan B, Rak J: Microvesicles: messengers and mediators of tumor progression. Cell Cycle 2009, 8:2014–2018
16. Jansen FH, Krijgsveld J, van Rijswijk A, van den Bemd GJ, van den Berg MS, van Weerden WM, Willemsen R, Dekker LJ, Luider TM, Jenster G: Exosomal secretion of cytoplasmic prostate cancer xenograft-derived proteins. Mol Cell Proteomics 2009, 8:1192–1205
17. Muralidharan-Chari V, Clancy J, Plou C, Romao M, Chavrier P, Raposo G, D'Souza-Schorey C: ARF6-regulated shedding of tumor cell-derived plasma membrane microvesicles. Curr Biol 2009, 19:1875–1885
18. Adam RM, Mukhopadhyay NK, Kim J, Di Vizio D, Cinar B, Boucher K, Solomon KR, Freeman MR: Cholesterol sensitivity of endogenous and myristoylated Akt. Cancer Res 2007, 67:6238–6246
19. Di Vizio D, Adam RM, Kim J, Kim R, Sotgia F, Williams T, Demichelis F, Solomon KR, Loda M, Rubin MA, Lisanti MP, Freeman MR: Caveolin-1 interacts with a lipid raft-associated population of fatty acid synthase. Cell Cycle 2008, 7:2257–2267
20. Powelka AM, Sun J, Li J, Gao M, Shaw LM, Sonnenberg A, Hsu VW: Stimulation-dependent recycling of integrin beta1 regulated by ARF6 and Rab11. Traffic 2004, 5:20–36
21. Wang S, Gao J, Lei Q, Rozengurt N, Pritchard C, Jiao J, Thomas GV, Li G, Roy-Burman P, Nelson PS, Liu X, Wu H: Prostate-specific deletion of the murine Pten tumor suppressor gene leads to metastatic prostate cancer. Cancer Cell 2003, 4:209–221
22. Chen Z, Trotman LC, Shaffer D, Lin HK, Dotan ZA, Niki M, Koutcher JA, Scher HI, Ludwig T, Gerald W, Cordon-Cardo C, Pandolfi PP: Crucial role of p53-dependent cellular senescence in suppression of Pten-deficient tumorigenesis. Nature 2005, 436:725–730
23. Braunhut SJ, Moses MA: Retinoids modulate endothelial cell production of matrix-degrading proteases and tissue inhibitors of metalloproteinases (TIMP). J Biol Chem 1994, 269:13472–13479
24. Ayala I, Baldassarre M, Giacchetti G, Caldieri G, Tete S, Luini A, Buccione R: Multiple regulatory inputs converge on cortactin to control invadopodia biogenesis and extracellular matrix degradation. J Cell Sci 2008, 121:369–378
25. Ramachandran A, Ranpura SA, Gong EM, Mulone M, Cannon GM Jr, Adam RM: An Akt- and Fra-1-dependent pathway mediates platelet-

derived growth factor-induced expression of thrombomodulin, a novel regulator of smooth muscle cell migration. Am J Pathol 2010, 177:119–131
26. Wersto RP, Chrest FJ, Leary JF, Morris C, Stetler-Stevenson MA, Gabrielson E: Doublet discrimination in DNA cell-cycle analysis. Cytometry 2001, 46:296–306
27. Ohi M, Li Y, Cheng Y, Walz T: Negative staining and image classification: powerful tools in modern electron microscopy. Biol Proced Online 2004, 6:23–34
28. Di Vizio D, Sotgia F, Williams TM, Hassan GS, Capozza F, Frank PG, Pestell RG, Loda M, Freeman MR, Lisanti MP: Caveolin-1 is required for the upregulation of fatty acid synthase (FASN), a tumor promoter, during prostate cancer progression. Cancer Biol Ther 2007, 6:1263–1268
29. Di Vizio D, Morello M, Sotgia F, Pestell RG, Freeman MR, Lisanti MP: An absence of stromal caveolin-1 is associated with advanced prostate cancer, metastatic disease and epithelial Akt activation. Cell Cycle 2009, 8:2420–2424
30. Mukhopadhyay NK, Kim J, Cinar B, Ramachandran A, Hager MH, Di Vizio D, Adam RM, Rubin MA, Raychaudhuri P, De Benedetti A, Freeman MR: Heterogeneous nuclear ribonucleoprotein K is a novel regulator of androgen receptor translation. Cancer Res 2009, 69: 2210–2218
31. Cinar B, Fang PK, Lutchman M, Di Vizio D, Adam RM, Pavlova N, Rubin MA, Yelick PC, Freeman MR: The pro-apoptotic kinase Mst1 and its caspase cleavage products are direct inhibitors of Akt1. EMBO J 2007, 26:4523–4534
32. Morishige M, Hashimoto S, Ogawa E, Toda Y, Kotani H, Hirose M, Wei S, Hashimoto A, Yamada A, Yano H, Mazaki Y, Kodama H, Nio Y, Manabe T, Wada H, Kobayashi H, Sabe H: GEP100 links epidermal growth factor receptor signalling to Arf6 activation to induce breast cancer invasion. Nat Cell Biol 2008, 10:85–92
33. Premont RT, Schmalzigaug R: Metastasis: wherefore arf thou? Curr Biol 2009, 19:R1036–R1038
34. Tomlins SA, Mehra R, Rhodes DR, Cao X, Wang L, Dhanasekaran SM, Kalyana-Sundaram S, Wei JT, Rubin MA, Pienta KJ, Shah RB, Chinnaiyan AM: Integrative molecular concept modeling of prostate cancer progression. Nat Genet 2007, 39:41–51
35. Yu YP, Landsittel D, Jing L, Nelson J, Ren B, Liu L, McDonald C, Thomas R, Dhir R, Finkelstein S, Michalopoulos G, Becich M, Luo JH: Gene expression alterations in prostate cancer predicting tumor aggression and preceding development of malignancy. J Clin Oncol 2004, 22:2790–2799
36. Holzbeierlein J, Lal P, LaTulippe E, Smith A, Satagopan J, Zhang L, Ryan C, Smith S, Scher H, Scardino P, Reuter V, Gerald WL: Gene expression analysis of human prostate carcinoma during hormonal therapy identifies androgen-responsive genes and mechanisms of therapy resistance. Am J Pathol 2004, 164:217–227
37. Lapointe J, Li C, Higgins JP, van de Rijn M, Bair E, Montgomery K, Ferrari M, Egevad L, Rayford W, Bergerheim U, Ekman P, DeMarzo AM, Tibshirani R, Botstein D, Brown PO, Brooks JD, Pollack JR: Gene expression profiling identifies clinically relevant subtypes of prostate cancer. Proc Natl Acad Sci U S A 2004, 101:811–816
38. Singh D, Febbo PG, Ross K, Jackson DG, Manola J, Ladd C, Tamayo P, Renshaw AA, D'Amico AV, Richie JP, Lander ES, Loda M, Kantoff PW, Golub TR, Sellers WR: Gene expression correlates of clinical prostate cancer behavior. Cancer Cell 2002, 1:203–209
39. Dudley AC, Khan ZA, Shih SC, Kang SY, Zwaans BM, Bischoff J, Klagsbrun M: Calcification of multipotent prostate tumor endothelium. Cancer Cell 2008, 14:201–211
40. Vanhecke E, Adriaenssens E, Verbeke S, Meignan S, Germain E, Berteaux N, Nurcombe V, Le Bourhis X, Hondermarck H: Brain-derived neurotrophic factor and neurotrophin-4/5 are expressed in breast cancer and can be targeted to inhibit tumor cell survival. Clin Cancer Res 2011, 17:1741–1752
41. Mi Z, Bhattacharya SD, Kim VM, Guo H, Talbot LJ, Kuo PC: Osteopontin promotes CCL5-mesenchymal stromal cell-mediated breast cancer metastasis. Carcinogenesis 2011, 32:477–487
42. Beauchemin N: The colorectal tumor microenvironment: the next decade. Cancer Microenviron 2011, 4:181–185
43. Keller H, Eggli P: Protrusive activity, cytoplasmic compartmentalization, and restriction rings in locomoting blebbing Walker carcinosarcoma cells are related to detachment of cortical actin from the plasma membrane. Cell Motil Cytoskeleton 1998, 41:181–193
44. Perner S, Svensson MA, Hossain RR, Day JR, Groskopf J, Slaughter RC, Jarleborn AR, Hofer MD, Kuefer R, Demichelis F, Rickman DS, Rubin MA: ERG rearrangement metastasis patterns in locally advanced prostate cancer. Urology 2010, 75:762–767
45. Tahir SA, Yang G, Ebara S, Timme TL, Satoh T, Li L, Goltsov A, Ittmann M, Morrisett JD, Thompson TC: Secreted caveolin-1 stimulates cell survival/clonal growth and contributes to metastasis in androgen-insensitive prostate cancer. Cancer Res 2001, 61:3882–3885
46. Williams TM, Hassan GS, Li J, Cohen AW, Medina F, Frank PG, Pestell RG, Di Vizio D, Loda M, Lisanti MP: Caveolin-1 promotes tumor progression in an autochthonous mouse model of prostate cancer: genetic ablation of Cav-1 delays advanced prostate tumor development in TRAMP mice. J Biol Chem 2005, 280:25134–25145
47. Duijvesz D, Luider T, Bangma CH, Jenster G: Exosomes as biomarker treasure chests for prostate cancer. Eur Urol 2011, 59:823–831
48. Bussolati B, Grange C, Camussi G: Tumor exploits alternative strategies to achieve vascularization. FASEB J 2011, 25:2874–2882
49. Chin YR, Toker A: Function of Akt/PKB signaling to cell motility, invasion and the tumor stroma in cancer. Cell Signal 2009, 21:470–476
50. Baldwin AL, Thurston G: Mechanics of endothelial cell architecture and vascular permeability. Crit Rev Biomed Eng 2001, 29:247–278
51. Park Y, Kitahara T, Urita T, Yoshida Y, Kato R: Expected clinical applications of circulating tumor cells in breast cancer. World J Clin Oncol 2011, 2:303–310